AGU PUBLICATIONS

JGR

Journal of Geophysical Research: Atmospheres

RESEARCH ARTICLE
10.1002/2016JD025819

Key Points:
- There is a strong lag relationship between June TOA RSR and September sea ice extent anomalies
- June TOA RSR anomalies are mainly contributed from Pacific Sector's surface condition variations and less affected by clouds
- TOA RSR is not properly represented by some of the reanalysis data sets, such as the ERA-Interim

Correspondence to:
Y. Zhan,
y.zhan@auckland.ac.nz

Citation:
Zhan, Y., and R. Davies (2017), September Arctic sea ice extent indicated by June reflected solar radiation, *J. Geophys. Res. Atmos.*, *122*, 2194–2202, doi:10.1002/2016JD025819.

Received 22 AUG 2016
Accepted 8 FEB 2017
Accepted article online 10 FEB 2017
Published online 21 FEB 2017

September Arctic sea ice extent indicated by June reflected solar radiation

Yizhe Zhan[1] **and Roger Davies**[1]

[1]Department of Physics, University of Auckland, Auckland, New Zealand

Abstract The predictability of the minimum sea ice extent (SIE) in the Arctic in September, especially for large anomaly years, is of strong current interest, given the rapid decline in sea ice amount. Our results show that June reflected solar radiation (RSR) is closely related to the underlying sea ice condition in that month and can be used to achieve September SIE predictions with good accuracy. The correlation coefficient between detrended June RSR and September SIE reaches 0.91 based on 16 year satellite observations, and the relatively high forecast skill using Modern-Era Retrospective analysis for Research and Applications Version 2 reanalysis data is similar to or better than other complex prediction models. The results confirm the particular importance of the early summer sea ice state and help to explain the abrupt declines of September SIE in the 21st century (2007 and 2012).

1. Introduction

The rapid decrease in the area of summer Arctic sea ice has been observed for several decades [*Serreze et al*., 2007; *Comiso et al*., 2008], along with thinner ice [*Giles et al*., 2008; *Kwok and Rothrock*, 2009], longer melt season [*Markus et al*., 2009], and the transformation to a mainly seasonal ice cover [*Rigor and Wallace*, 2004; *Maslanik et al*., 2007, 2011]. Arctic sea ice extent reaches a minimum in September, with an area that has decreased dramatically from more than 7 million km^2 in the 1980s to less than 5 million km^2 in the past 5 years. However, most of the current climate models do not correctly capture this significant decrease [*Stroeve et al*., 2012]. They range so widely in their September sea ice extents (SIEs) that a better understanding of the observed sea ice loss presents a "grand challenge" for climate science [*Kattsov et al*., 2010], especially for years of large September SIE anomalies [*Stroeve et al*., 2014].

Although the evolution of sea ice physical properties has been extensively studied, prediction of detrended SIE with lead times of 3 months and longer has not yet been promising [*Lindsay et al*., 2008; *Blanchard-Wrigglesworth et al*., 2011]. For SIE itself, no significant correlation was found between early summer and September SIE [*Schröder et al*., 2014] and the autocorrelation of detrended anomalies becomes essentially zero for 1 year lag [*Serreze and Stroeve*, 2015]. Additionally, forecasts from the state-of-the-art coupled atmosphere-ocean sea ice models [*Chevallier et al*., 2013; *Sigmond et al*., 2013; *Wang et al*., 2013] do not show better results than statistical models [*Kapsch et al*., 2014; *Schröder et al*., 2014], indicating that our understanding regarding the controlling factors of sea ice melt may still be insufficient. As a result, a number of studies have attempted to relate sea ice reduction to anomalous atmospheric and surface conditions. Based on the ERA-Interim reanalysis data set, *Kapsch et al*. [2014] suggested that correlation coefficients (CCs) of 0.5 could be achieved between observed and predicted September sea ice concentration by considering the spring-time downwelling longwave radiation and water vapor. By using the spring melt pond fraction, *Schröder et al*. [2014] achieved an anomaly correlation coefficient (ACC) of up to 0.65. Regardless of the fact that they are still not capable of predicting September SIE with large negative anomalies [*Kapsch et al*., 2014], these strong correlations hint that a significant factor during the early melt season affects the subsequent summer ice retreat [*Perovich et al*., 2007]. More recently, *Choi et al*. [2014] suggested that the June sunlight drives Arctic sea ice loss in the late summer. A high, significant correlation was found between deseasonalized June absorbed solar radiation (ASR) and late summer sea ice. However, neither detrended relationship nor predictive skill was analysed.

Here we examine the relationship between September SIE and June top-of-atmosphere (TOA) reflected solar radiation (RSR, equivalent to ASR) by using both satellite observations and reanalysis data sets. While the satellite data (2000–2015) provide a more direct relationship, reanalysis data (1979–2015) offer us a much longer period to evaluate the potential for a skilful forecast. We note that, as a good representative of

underlying surface state (albedo), June RSR shows a robust 3 month lag correlation with September SIE, especially for the years with an abrupt decrease in sea ice extent (2007 and 2012). Finally, we quantify the hindcast/forecast skills of using June RSR for September SIE predictions.

2. Data and Methods

In this study, monthly data sets from both satellite observations and reanalysis products were area-weighted and averaged over the Arctic Ocean poleward of 70°N. SIE, defined as the summed area of all pixels that are each at least 15% covered by sea ice with a spatial resolution of 25 km, is calculated from sea ice concentration data set (sea ice concentrations from Nimbus 7 scanning multichannel microwave radiometer and DMSP Special Sensor Microwave Imager (SSM/I) SSMIS Passive Microwave Data Special Sensor Microwave Imager/Sounder Version 1) provided by the National Snow and Ice Data Center (NSIDC) [*Cavalieri et al*., 1996] with a reported uncertainty of ± 15 % during melt seasons [*Cavalieri et al*., 1992]. NSIDC provides a consistent combination of records from a series of passive microwave sensors and is available for the period of 1979–2015.

The monthly gridded radiation data (1° × 1° spatial resolution) are obtained from both satellite and reanalysis data sets, which are available up to present day. Being widely used in Arctic studies [e.g., *Porter et al*., 2010; *Choi et al*., 2014; *Kim et al*., 2016], Clouds and the Earth's Radiant Energy System (CERES) is regarded as one of the best spaceborne instruments measuring TOA radiation. However, *Kato and Loeb* [2005] found that CERES shortwave Angular Distribution Models encounter a larger uncertainty in the polar regions compared to the other areas. Thus, we also considered the TOA-RSR data set from the Multiangle Imaging Spectroradiometer (MISR). Both instruments are onboard NASA's Terra satellite and provide daily coverage of the entire Arctic but use independent approaches for scene identification and RSR retrieval. While CERES adopts a Moderate Resolution Imaging Spectroradiometer radiance-based cloud mask, MISR takes advantage of its stereoscopic-derived cloud mask. Note that MISR produces three kinds of albedo products (local, restrictive, and expansive albedo) in its monthly component global albedo product (MISR_AM1_CGAL_F04_0024). The restrictive albedo is chosen for this study because it is closer to the Earth Radiation Budget Experiment (ERBE) or CERES definition of albedo [*Sun et al*., 2006], which is confined to the reflected flux emanating from the reflecting surfaces within the region. The CERES Energy Balanced And Filled (EBAF) data set (CERES_EBAF) Edition 2.8 is selected for the same purpose. It is an upgraded version of the CERES Synoptic Radiative Fluxes and Clouds data set that constrains the global net energy to the ocean heat storage term [*Loeb et al*., 2009]. The uncertainty in the CERES observed reflected shortwave flux at TOA is ~5% [*CERES*, 2014], and the consistency of retrieved cloud albedo between CERES and MISR is ~4% over the Arctic (not shown). Moreover, since CERES had a data outage for half of June in 2001, which therefore caused a much larger monthly mean RSR, this particular month has been excluded from analysis. To extend our analysis backward, we used the RSR data from the NOAA-9/10 Earth Radiation Budget Experiment (ERBE scanner, 1985–1989). ERBE can be treated as a predecessor of CERES with a coarser spatial resolution (40 km for footprint data and 2.5° × 2.5° spatial resolution for monthly data). While we have confidence in the latest RSR products, the previous data set allows us to trace back to gain confidence in the relationship. In addition to the satellite retrievals, we checked RSR data from two state-of-the-art reanalysis data sets, which are ERA-Interim reanalysis (ERA) from European Centre of Medium-Range Weather Forecasts (ECMWF) [*Dee et al*., 2011] and Modern-Era Retrospective analysis for Research and Applications Version 2 reanalysis (MERRA2) from NASA [*Rienecker et al*., 2011]. All the data have a 1° × 1° horizontal resolution and are available for the period of 1979–2015 (ERA) and 1980–2015 (MERRA2).

While quantifying the lag correlation between June RSR and September SIE, it should be noted that all data are detrended to focus on the interannual variability. Two different linear trends, with fits over CERES/MISR period (2000–2015) and MERRA2 period (1980–2015), were subtracted from the corresponding RSR and SIE data sets, respectively. As the number of satellite-based RSR is limited ($n = 15$ for June), we only checked the Pearson correlation coefficient for the detrended time series of June RSR with the detrended time series of September ice extent. A statistical prediction model based on all available data (hindcast) is evaluated by calculating the corresponding prediction error variance (σ^2_{err}).

Meanwhile, the RSR from the reanalysis data set was also used to assess the forecast performance. We first used 5 year (1980–1984) detrended anomalies of June TOA RSR and September SIE to establish the first

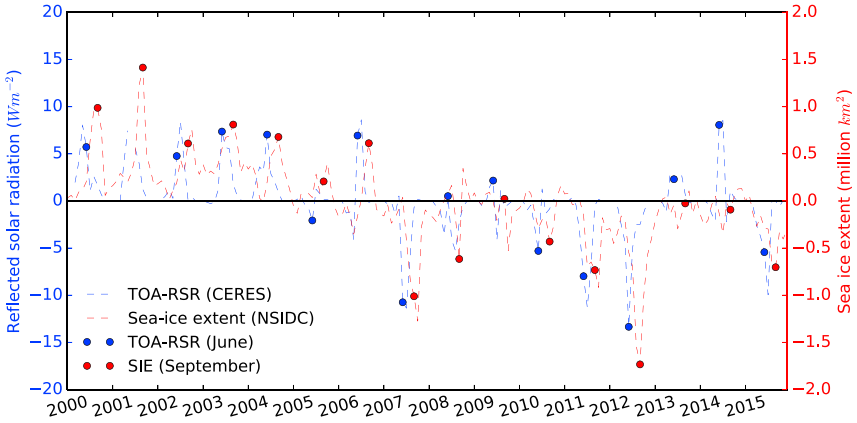

Figure 1. Time series of deseasonalized monthly anomalies of sea ice extent (SIE) and top-of-atmosphere reflected solar radiation (RSR) from 2000 to 2015. SIE is from NSIDC, and RSR is from CERES-EBAF data set. Note that all monthly values are area averaged over Arctic Ocean (70°N–90°N).

linear regression equation. This equation is then applied to the following detrended June TOA-RSR anomaly, resulting in an estimation of the corresponding September SIE anomaly. The final September SIE is the sum of the SIE anomaly and the SIE estimated from the trend. Afterward, data only from previous years are used to calculate the linear regression and the error of the 31 forecast years (1985–2015). To make a direct comparison with previous studies [*Kapsch et al.*, 2014; *Schröder et al.*, 2014], we calculated variances of detrended observed ice extent (σ^2_{ref}) and forecast error (σ^2_{ferr}). The forecast skill (S) is then determined by

$$S = 1 - \frac{\sigma^2_{\mathrm{ferr}}}{\sigma^2_{\mathrm{ref}}} \tag{1}$$

In addition to the robust statistical models, making real September SIE prediction requires relatively short data latency. In general, most of operational (final status) data sets have latencies of about 2–3 weeks (MERRA2) through to several months (CERES and MISR) after the completion of a month, which strongly restrict the timely September SIE prediction. However, MISR also provides a first-look TOA albedo product (*MISR_AM1_CGAL_1_DEG_FIRSTLOOK*), which is usually released ~2 days after each month and is sufficiently close to its final-status product (root-mean-square error ~0.1%). Thus, it can be used to make timely September SIE predictions.

3. Results

Previous studies indicated that it is difficult to do the prediction of detrended September SIE with lead times of 3 months and longer [*Lindsay et al.*, 2008; *Blanchard-Wrigglesworth et al.*, 2011] and even harder in the large anomaly years [*Kapsch et al.*, 2014]. Here we show the existence of a robust 3 month lag correlation between September sea ice extent and June TOA reflected solar radiation (equivalent to the TOA absorbed solar radiation or albedo). This correlation may benefit the future September SIE predictions.

3.1. Lag Relationship Analysis

Figure 1 shows the time series of deseasonalized reflected solar radiation (blue) and sea ice extent (red) from 2000 to 2015. Except for 3 years (2005, 2008, and 2014) with small September SIE anomaly, the 3 month leads of RSR to SIE are consistently observed over the past 16 years: each June RSR anomaly (blue dot) is followed by an SIE anomaly (red dot) in the subsequent September with the same sign and similar relative magnitude. Meanwhile, for years with particularly low September SIE (2007, 2012, and 2015), there are correspondingly large negative RSR anomalies only in the previous June. This is consistent with the results of *Choi et al.* [2014], who found that the largest covariance between late summer SIE and total absorbed solar radiation (ASR) was in June. Note that we used deseasonalized anomalies here. As a result, the 3 month lagged correlation between June RSR and September SIE is not a consequence of the seasonal cycle [*Choi et al.*, 2014]. Instead, it shows a promising potential to provide September SIE predictions, especially for

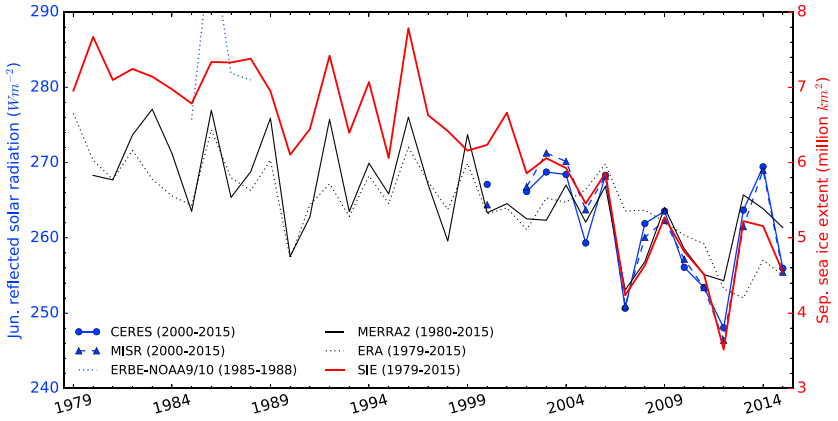

Figure 2. Time series of September sea ice extent and June reflected solar radiation from various data sources. The blue and black lines represent June reflected solar radiation data sets, and the red line represents September sea ice extent.

the large anomaly years. Therefore, the RSR in June seems to be an indicator of the sea ice state in the subsequent September.

To gain further confidence in the relationship between June RSR and September SIE, we expanded the time range back to 1979 and added additional RSR data from the ERBE and reanalysis data sets (Figure 2). The RSR scales of both reanalysis and MISR data sets have been adjusted to the CERES scale based on their overlapped years. We show absolute values here because only 4 years of satellite-retrieved RSR data were available in 1980s. The September SIE was high in the 1980s, when ERBE also showed a large June RSR at ~280 W/m^2.

Nevertheless, both reanalysis data sets did not show such high RSR values. This could be a consequence of using predescribed climatological sea ice albedo [*Karlsson and Svensson*, 2013]. The progressive replacement of multiyear sea ice by seasonal sea ice [*Overpeck et al*., 2005] results in a shallower snow cover and flatter topography that would help pond formation [*Perovich and Polashenski*, 2012] and lead to a significant difference of summer sea ice albedo evolution starting in late May [*Perovich et al*., 2002; *Perovich and Polashenski*, 2012]. Thus, even though the reanalysis data sets either directly adopt or assimilate satellite-retrieved ice concentrations [*Kapsch et al*., 2013; *Bosilovich et al*., 2015], they may still overlook the changes of the sea ice albedo, underestimating the TOA-RSR trends. Although ERA-Interim reanalysis is one of the best data sets representing the Arctic climate [*Lindsay et al*., 2014] and had been extensively used in the previous studies [*Kapsch et al*., 2013, 2014], it shows little consistency of RSR with respect to CERES observations for their overlapped time period (CC = 0.26). In comparison, MERRA2 indicates a significant correlation of CC = 0.88 for the same time interval. This could be a consequence of the much higher and more variable cloud fraction in ERA-Interim reanalysis data set. A spurious increase in cloud amount would shield more of the underlying surface, reducing the difference in TOA-RSR between the dark ocean and the bright sea ice, possibly causing the unrealistic TOA-RSR provided by the ERA-Interim. The different results from the two reanalysis data sets indicate that radiation data from any reanalysis data set should be carefully examined before applying it to Arctic studies. Thus, we selected MERRA2 to examine the forecast skill in the following study.

To quantify the relationship between June RSR and SIE in the subsequent September, Figure 3a shows the detrended September SIE anomalies and the June RSR anomalies from both CERES and MISR for their time series. It is important to recall that the methodologies of retrieving top-of-atmosphere RSR are fundamentally different between the two instruments, therefore giving us greater confidence in their retrievals since both of the instruments correspond quite well. Moreover, the fluctuation of June RSR anomalies correlates well with the sea ice extent anomalies 3 months later; in both sign and magnitude, implying the September SIE anomaly could be sensitive to the physical state anomalies that are captured by the RSR anomaly in June. Figure 3b shows the scatterplot of all the anomalies. It is clear that there is a highly significant positive correlation (P value < 0.00001 for both data sets) between the June RSR anomaly and the September SIE anomaly. The anomaly correlation coefficient reaches up to 0.91 (0.65 to 0.98 at the 99% confidence level) for the 15 year CERES/MISR TOA-RSR data set, which is significantly higher than other relationships that had been discovered so far [*Kapsch et al*., 2014; *Schröder et al*., 2014; *Guemas et al*., 2016].

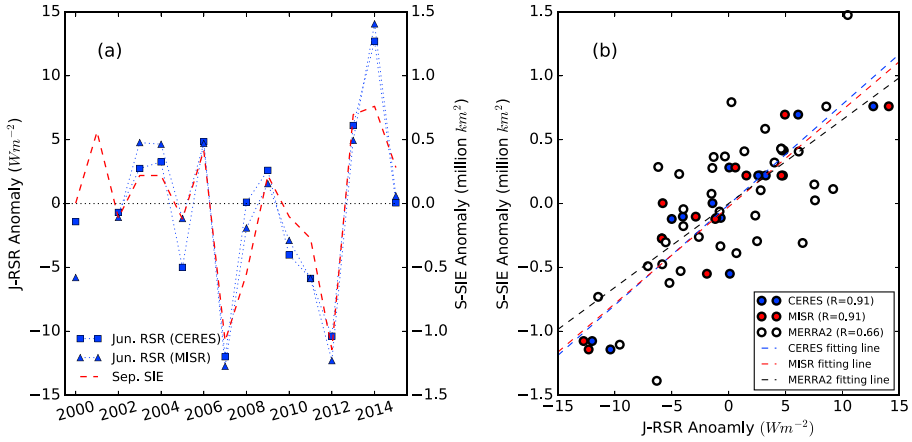

Figure 3. Relationship between detrended June reflected solar radiation and September sea ice extent. (a) Anomaly between CERES (MISR) derived reflected solar radiation and SSM/I retrieved sea ice extent. (b) Scatter plot for the June reflected solar radiation and the September sea ice extent anomaly. Linear regression lines have been fit to the data (dashed lines).

It might be argued that such a high correlation could be due to only 15 years of available satellite observations. As a result, we also considered anomalies from 36 years of MERRA2 reanalysis, which shows better consistency than ERA-Interim with respect to CERES. The highly significant correlation (P value < 0.00001) with a slightly lower coefficient of 0.66 (0.33 to 0.85 at the 99% confidence level) confirms the robust relationship. In addition, the three fitting lines (Figure 3b) are similar, implying that the relationship is stable during the past several decades regardless of different data sets. Regarding the extreme years, the two largest negative anomaly years (2012 and 2007) of September SIE also correspond to the two lowest June RSR anomalies. Thus, the June RSR anomaly could have the potential of predicting exceptionally low September SIE.

The reason for the significant lag relationship between detrended June RSR and September SIE anomalies can likely be explained by the following physical mechanism: in the early summer, ice is mainly melted from the top due to surface heat flux [*Steele et al*., 2010], which is dominated by shortwave radiation. As the cumulative solar heat input to the ice greatly depends on ice albedo since June [*Perovich and Polashenski*, 2012], an anomalous June surface albedo by any factor would significantly impact the subsequent ice evolution by positive ice-albedo feedback. Similarly, *Schröder et al*. [2014] found a strong correlation between late spring (May–June) pond fraction and September ice extent. For an invariant solar constant, the RSR anomaly is equivalent to the ASR anomaly (ΔASR_{TOA}), which is a combination of anomalous ASR by the atmosphere (ΔASR_{atm}) and by the surface (ΔASR_{sfc}). The latter term can further be decomposed as

$$\Delta ASR_{sfc} = (1-\alpha_{sfc})\times\Delta SWD_{sfc} + SWD_{sfc}\times(1-\Delta\alpha_{sfc}) + o \quad (2)$$

where α_{sfc} is the surface albedo and SWD_{sfc} is the downwellling shortwave radiation. As both SWD_{sfc} and surface upwelling shortwave radiation are available in the CERES EBAF data set, α_{sfc} can be calculated for each 1° grid. Δ denotes the deseasonalized monthly anomaly and o the residual item that is relatively small. Because of cloud impacts on both ASR_{atm} and SWD_{sfc}, the atmospheric contribution can be written as

$$CON_{atm} = \Delta ASR_{atm} + (1-\alpha_{sfc})\times\Delta SWD_{sfc} \quad (3)$$

and the surface contribution as $CON_{sfc} = (1-\Delta\alpha_{sfc})\times SWD_{sfc}$. Therefore, the deseasonalized ASR anomaly for a single column can be written as $\Delta ASR_{TOA} = CON_{atm} + CON_{sfc} + o$.

Based on the 16 year deseasonalized CERES EBAF data set (excluding June 2001), we separated the Arctic Ocean into five subregions (Figure 4) and calculated the variance of each component for 6 months from April to September (Figure 5). It is clear that the surface has the larger contribution within all subregions for June ASR anomalies. Particularly, most of the surface contribution originated from Regions I and IV, where the majority of the September sea ice extent variations were found. For the other months, although overall contributions from the surface are all larger than they are from the atmosphere, these anomalies either originated from Region III (May) or were strongly affected by the atmosphere (April, July, and August).

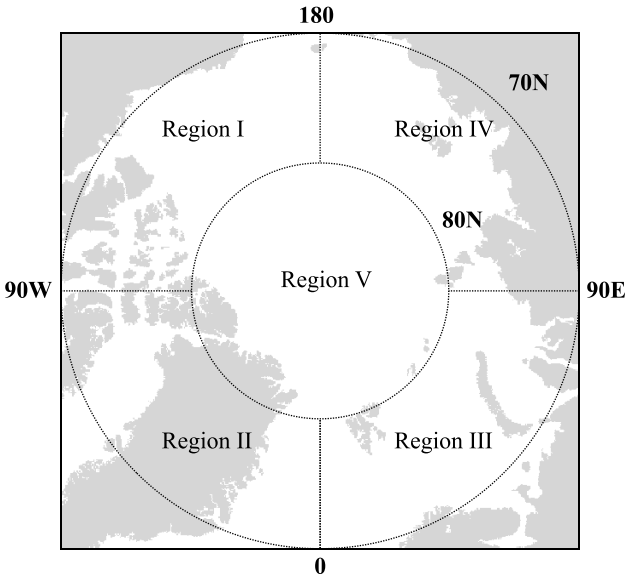

Figure 4. An illustration of five studied subregions of Arctic Ocean.

Thus, due to the merit of representing the Pacific Sector's (Regions I and IV) surface albedo variation and being least affected by the atmosphere, June ASR (RSR) should be a good indicator for the subsequent September SIE.

3.2. September Sea Ice Prediction

To investigate the potential of using June RSR for Arctic September sea ice prediction, both hindcast and forecast models were analysed. For the hindcast, we first used the whole available data period of the detrended June RSR and September SIE to derive the linear regression line, which is then applied to estimate September SIE from June RSR. This was done separately for MERRA2, CERES, and MISR. To test the usage of TOA-RSR for real forecasts of Arctic September sea ice, a forecast method was developed by only using MERRA2 data from all previous years. Figure 6 shows the comparison between predicted and observed September SIE for both the anomaly (Figure 6a) and absolute values (Figure 6b). The root-mean-square prediction errors are relatively small for all three hindcasts, ranging from $\sigma_{err} = 0.22$ million km^2 for CERES/MISR to $\sigma_{err} = 0.39$ million km^2 for MERRA2. This is comparable to the results of *Schröder et al.* [2014], who achieved a prediction error of 0.36 million km^2 based on the pond fraction from 1 May to 25 June.

For the forecast experiment based on the 36 year MERRA2 reanalysis data set, we achieved anomaly correlation coefficients ACC = 0.61. This value is similar to or better than the recent studies using either statistical

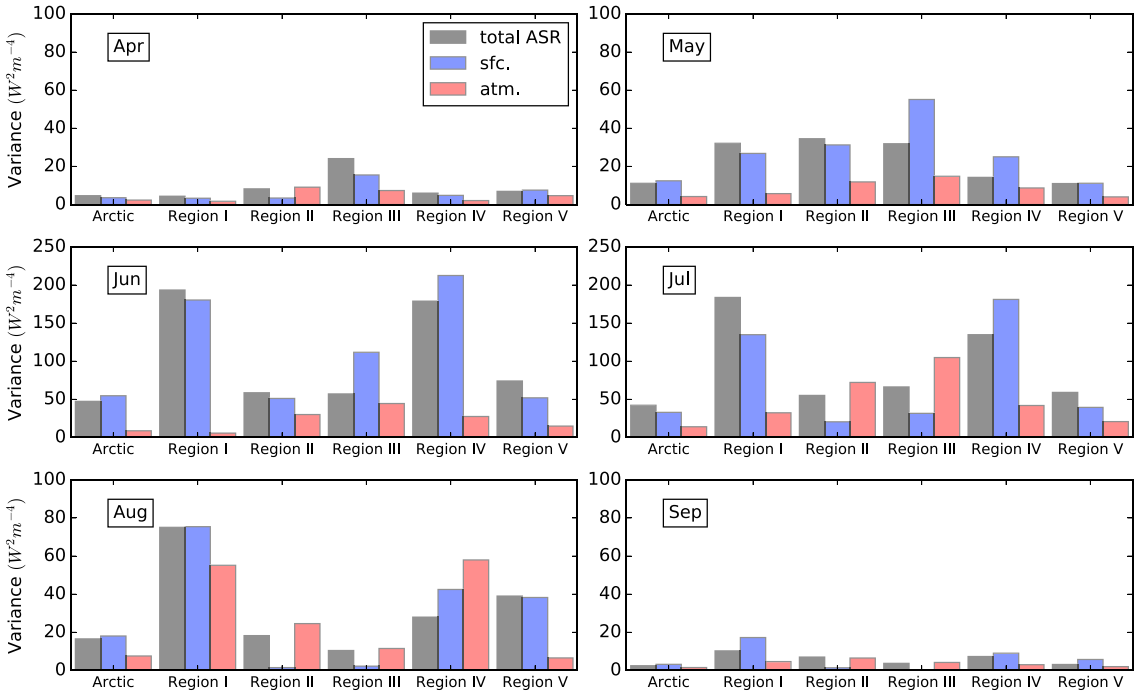

Figure 5. Variances of deseasonalized ASR anomaly components for each region over the Arctic Ocean. Data are from CERES-EBAF data set within the Arctic (70 ° N northward) for the period of 2000–2015 (excluding June 2001). Boundaries of each region are shown in Figure 4.

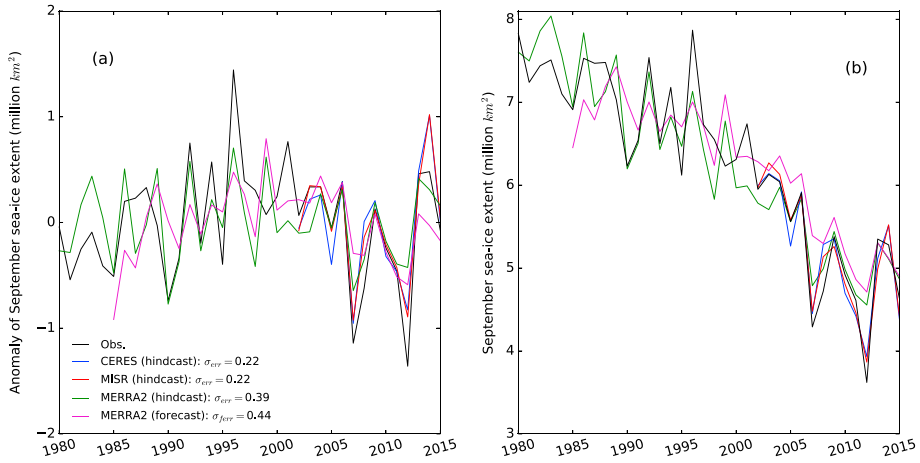

Figure 6. The observed (NSIDC) and predicted September sea ice extent anomalies from the (a) trend line and (b) absolute values from MERRA2, CERES, and MISR. σ_{err} is the root-mean-square prediction error in million km^2.

methods [*Kapsch et al*., 2014; *Schröder et al*., 2014] or complex prediction models [*Chevallier et al*., 2013; *Day et al*., 2014]. The corresponding forecast error $\sigma_{ferr} = 0.44$ million km^2 is identical to the September ice forecast based on pond fraction from 1 May to 25 June [*Schröder et al*., 2014]. Considering the detrended observed SIE standard deviation $\sigma_{ref} = 0.56$ million km^2, the forecast skill $S = 0.38$ (equation (1)) is close to the skill of 0.41 achieved by *Schröder et al.* [2014] and much better than the negative skill from statistical forecasts [*Lindsay et al*., 2008]. For the year of 2015, hindcasts from CERES and MISR estimated 4.4 ± 0.2 million km^2 and both hindcast and forecast of MERRA2 predict the same September SIE of 4.8 ± 0.4 million km^2, which are very close to the observation of 4.63 million km^2. By comparison, the median value of 35 Arctic SIE predictions presented at the Arctic Sea Ice Outlook web page (https://www.arcus.org/sipn/sea-ice-outlook/2015/july) is 5.0 million km^2.

4. Discussion and Conclusion

In this study, a significant 3 month lag correlation between June RSR and September SIE has been noted over the last few decades. This result agrees with *Choi et al.* [2014], who found that the largest covariance between late summer SIE and TOA-ASR (equivalent to RSR) was in June. However, they attributed the June ASR anomaly mainly to the cloud shielding effect, which might result from their use of a single-layer cloud model to retrieve the cloud albedo time series data. This approach should be appropriate when the underlying surface albedo has small variation. However, the albedo of sea ice varies so much (from as low as 0.15 for ponded ice up to 0.95 for snow-covered ice [*Schröder et al*., 2014]) that the change of "cloud albedo" could also be greatly affected by the surface albedos. Also based on the CERES data set, we decomposed the ASR anomaly into its surface and atmospheric contributions. We found that it is the variation of underlying surface albedo within the Pacific Sector of the Arctic that contributes to the majority of overall June ASR anomalies, which is distinct from the conclusion made by *Choi et al.* [2014]. Nevertheless, it does not mean that the atmosphere (cloud) is not important in Arctic: cloud variation inserts an equivalent impact on the ASR variance as the surface in April and dominates the ASR variance of the Atlantic Sector from July to September.

Like other statistical models of Arctic seasonal ice prediction using the preseasonal parameters [*Kapsch et al*., 2014; *Schröder et al*., 2014], the prediction accuracy is strongly limited by the chaotic nature of the atmosphere so that it is fundamentally impossible to estimate a perfect September SIE without considering the impact of the atmospheric and oceanic processes in July–September. For example, winds affect the sea ice by forcing ice motion northward and advecting heat and moisture to high latitudes [*Zhang et al*., 2008]. An anomalous increase in the oceanic heat transport can enhance the ablation of the ice from the bottom, which could also contribute to the dramatic decline of September SIE in 2007 [*Woodgate et al*., 2010]. Furthermore, studies have shown that the increased strength and size of cyclones in the melt season may accelerate the rate of decrease in ice extent [*Comiso et al*., 2008; *Simmonds and Keay*, 2009; *Parkinson and Comiso*, 2013]. These factors may each change the September SIE to some extent, contributing to the prediction errors of

using June RSR alone. Despite the simple statistical approach proposed in this study, the predictive skills for both hindcast and forecast are comparable or even better than other forecast models [e.g., *Chevallier et al*., 2013; *Kapsch et al*., 2014; *Schröder et al*., 2014], underlining particular importance of the early summer ice state for September SIE predictions. Thus, the close relationship between sea ice status and TOA-RSR anomaly in June may help the insufficient initial conditions in the complex sea ice prediction models, and the 3 month lag correlation of TOA-RSR and SIE could also be used as a first-order constraint for the modeled results. In addition, RSR can be retrieved from satellite observations directly (CERES and MISR) with good accuracy, which ensures the stability of using RSR itself as a predictor for September SIE prediction. However, it should also be noted that RSR is not properly represented by some of the reanalysis data sets, such as ERA-Interim.

Acknowledgments

This research was supported by subcontract 1460339 between the California Institute of Technology/Jet Propulsion Laboratory and the University of Auckland and the sponsorship from the Chinese Scholarship Council. Sea ice concentration data were provided by the National Snow and Ice Data Center (http://nsidc.org/data/NSIDC-0051). MISR, CERES, and ERBE data were obtained from the NASA Langley Research Center Atmospheric Science Data Center (https://eosweb.larc.nasa.gov/). The ERA-Interim reanalysis was obtained from the ECMWF data server (http://apps.ecmwf.int/datasets/data/interim-full-mnth). The MERRA2 data were provided by the Global Modelling and Assimilation Office (GMAO) and the GES DISC for the dissemination (http://disc.sci.gsfc.nasa.gov/daac-bin/FTPSubset2.pl).

References

Blanchard-Wrigglesworth, E., K. C. Armour, C. M. Bitz, and E. Deweaver (2011), Persistence and inherent predictability of arctic sea ice in a GCM ensemble and observations, *J. Clim.*, *24*(1), 231–250, doi:10.1175/2010JCLI3775.1.

Bosilovich, M., et al. (2015), MERRA-2: Initial evaluation of the climate, *NASA Tech. Rep. Ser. on Global Model. and Data Assimilation*, NASA/TM-2015, 104606.

Cavalieri, D. J., et al. (1992), NASA sea ice validation program for the Defense Meteorological Satellite Program Special Sensor Microwave Imager, *Final Rep. NASA Tech. Mem*., 104559.

Cavalieri, D. J., C. L. Parkinson, P. Gloersen, and H. Zwally (1996), *Sea Ice Concentrations From Nimbus-7 SMMR and DMSP SSM/I-SSMIS Passive Microwave Data (1979–2015)*, Natl. Snow and Ice Data Cent., Digital media, Boulder, Colo., doi:10.5067/8GQ8LZQVL0VL.

CERES (2014), CERES EBAF Ed2.8 data quality summary. [Available at https://ceres.larc.nasa.gov/documents/DQ_summaries/CERES_EBAF_Ed2.8_DQS.pdf.]

Chevallier, M., D. S. Y. Mélia, A. Voldoire, M. Déqué, and G. Garric (2013), Seasonal forecasts of the pan-arctic sea ice extent using a GCM-based seasonal prediction system, *J. Clim.*, *26*(16), 6092–6104, doi:10.1175/JCLI-D-12-00612.1.

Choi, Y. S., B. M. Kim, S. K. Hur, S. J. Kim, J. H. Kim, and C. H. Ho (2014), Connecting early summer cloud-controlled sunlight and late summer sea ice in the Arctic, *J. Geophys. Res. Atmos.*, *119*, 11,087–11,099, doi:10.1002/2014JD022013.

Comiso, J. C., C. L. Parkinson, R. Gersten, and L. Stock (2008), Accelerated decline in the Arctic sea ice cover, *Geophys. Res. Lett.*, *35*, L01703, doi:10.1029/2007GL031972.

Day, J. J., S. Tietsche, and E. Hawkins (2014), Pan-arctic and regional sea ice predictability: Initialization month dependence, *J. Clim.*, *27*(12), 4371–4390, doi:10.1175/JCLI-D-13-00614.1.

Dee, D. P., et al. (2011), The ERA-Interim reanalysis: Configuration and performance of the data assimilation system, *Q. J. R. Meteorol. Soc.*, *137*(656), 553–597, doi:10.1002/qj.828.

Giles, K. A., S. W. Laxon, and A. L. Ridout (2008), Circumpolar thinning of Arctic sea ice following the 2007 record ice extent minimum, *Geophys. Res. Lett.*, *35*, L22502, doi:10.1029/2008GL035710.

Guemas, V., et al. (2016), A review on Arctic sea-ice predictability and prediction on seasonal to decadal time-scales, *Q. J. R. Meteorol. Soc.*, *142*(695), 546–561, doi:10.1002/qj.2401.

Kapsch, M. L., R. G. Graversen, T. Economou, and M. Tjernström (2014), The importance of spring atmospheric conditions for predictions of the Arctic summer sea ice extent, *Geophys. Res. Lett.*, *41*, 5288–5296, doi:10.1002/2014GL060826.

Kapsch, M.-L., R. G. Graversen, and M. Tjernström (2013), Springtime atmospheric energy transport and the control of Arctic summer sea-ice extent, *Nat. Clim. Change*, *3*(8), 744–748, doi:10.1038/nclimate1884.

Karlsson, J., and G. Svensson (2013), Consequences of poor representation of Arctic sea-ice albedo and cloud-radiation interactions in the CMIP5 model ensemble, *Geophys. Res. Lett.*, *40*, 4374–4379, doi:10.1002/grl.50768.

Kato, S., and N. G. Loeb (2005), Top-of-atmosphere shortwave broadband observed radiance and estimated irradiance over polar regions from Clouds and the Earth's Radiant Energy System (CERES) instruments on Terra, *J. Geophys. Res.*, *110*, D07202, doi:10.1029/2004JD005308.

Kattsov, V., V. E. Ryabinin, J. E. Overland, M. C. Serreze, M. Visbeck, J. E. Walsh, W. Meier, and X. Zhang (2010), Arctic sea-ice changes: A grand challenge of climate science, *J. Glaciol.*, *56*(200), 1115–1121, doi:10.3189/002214311796406176.

Kim, Y., H.-R. Kim, Y.-S. Choi, W. Kim, and H.-S. Kim (2016), Development of statistical seasonal prediction models of Arctic sea ice concentration using CERES absorbed solar radiation, *Asia-Pacific J. Atmos. Sci.*, *52*(5), 467–477, doi:10.1007/s13143-016-0031-y.

Kwok, R., and D. A. Rothrock (2009), Decline in Arctic sea ice thickness from submarine and ICESat records: 1958–2008, *Geophys. Res. Lett.*, *36*, L15501, doi:10.1029/2009GL039035.

Lindsay, R., M. Wensnahan, A. Schweiger, and J. Zhang (2014), Evaluation of seven different atmospheric reanalysis products in the arctic, *J. Clim.*, *27*(7), 2588–2606, doi:10.1175/JCLI-D-13-00014.

Lindsay, R. W., J. Zhang, A. J. Schweiger, and M. A. Steele (2008), Seasonal predictions of ice extent in the Arctic Ocean, *J. Geophys. Res.*, *113*, C02023, doi:10.1029/2007JC004259.

Loeb, N. G., B. A. Wielicki, D. R. Doelling, G. L. Smith, D. F. Keyes, S. Kato, N. Manalo-Smith, and T. Wong (2009), Toward optimal closure of the Earth's top-of-atmosphere radiation budget, *J. Clim.*, *22*(3), 748–766, doi:10.1175/2008JCLI2637.1.

Markus, T., J. C. Stroeve, and J. Miller (2009), Recent changes in Arctic sea ice melt onset, freezeup, and melt season length, *J. Geophys. Res.*, *114*, C12024, doi:10.1029/2009JC005436.

Maslanik, J., J. Stroeve, C. Fowler, and W. Emery (2011), Distribution and trends in Arctic sea ice age through spring 2011, *Geophys. Res. Lett.*, *38*, L13502, doi:10.1029/2011GL047735.

Maslanik, J. A., C. Fowler, J. Stroeve, S. Drobot, J. Zwally, D. Yi, and W. Emery (2007), A younger, thinner Arctic ice cover: Increased potential for rapid, extensive sea-ice loss, *Geophys. Res. Lett.*, *34*, L24501, doi:10.1029/2007GL032043.

Overpeck, J. T., et al. (2005), Arctic system on trajectory to new, seasonally ice-free state, *Eos Trans. Am. Geophys. Union*, *86*(34), 309, doi:10.1029/2005EO340001.

Parkinson, C. L., and J. C. Comiso (2013), On the 2012 record low Arctic sea ice cover: Combined impact of preconditioning and an August storm, *Geophys. Res. Lett.*, *40*, 1356–1361, doi:10.1002/grl.50349.

Perovich, D. K., and C. Polashenski (2012), Albedo evolution of seasonal Arctic sea ice, *Geophys. Res. Lett.*, *39*, L08501, doi:10.1029/2012GL051432.

Perovich, D. K., T. C. Grenfell, B. Light, and P. V. Hobbs (2002), Seasonal evolution of the albedo of multiyear Arctic sea ice, *J. Geophys. Res.*, *107*(C10), 8044, doi:10.1029/2000JC000438.

Perovich, D. K., S. V. Nghiem, T. Markus, and A. Schweiger (2007), Seasonal evolution and interannual variability of the local solar energy absorbed by the Arctic sea ice-ocean system, *J. Geophys. Res.*, *112*, C03005, doi:10.1029/2006JC003558.

Porter, D. F., J. J. Cassano, M. C. Serreze, and D. N. Kindig (2010), New estimates of the large-scale Arctic atmospheric energy budget, *J. Geophys. Res.*, *115*, D08108, doi:10.1029/2009JD012653.

Rienecker, M. M., et al. (2011), MERRA: NASA's modern-era retrospective analysis for research and applications, *J. Clim.*, *24*(14), 3624–3648, doi:10.1175/JCLI-D-11-00015.1.

Rigor, I. G., and J. M. Wallace (2004), Variations in the age of Arctic sea-ice and summer sea-ice extent, *Geophys. Res. Lett.*, *31*, L09401, doi:10.1029/2004GL019492.

Schröder, D., D. L. Feltham, D. Flocco, and M. Tsamados (2014), September Arctic sea-ice minimum predicted by spring melt-pond fraction, *Nat. Clim. Change*, *4*(5), 353–357, doi:10.1038/nclimate2203.

Serreze, M. C., and J. Stroeve (2015), Arctic sea ice trends, variability and implications for seasonal ice forecasting, *Phil. Trans. R. Soc. A*, *373*, 20140159, doi:10.1098/rsta.2014.0159.

Serreze, M. C., M. M. Holland, and J. Stroeve (2007), Perspectives on the Arctic's shrinking sea-ice cover, *Science*, *315*(5818), 1533–1536, doi:10.1126/science.1139426.

Sigmond, M., J. C. Fyfe, G. M. Flato, V. V. Kharin, and W. J. Merryfield (2013), Seasonal forecast skill of Arctic sea ice area in a dynamical forecast system, *Geophys. Res. Lett.*, *40*, 529–534, doi:10.1002/grl.50129.

Simmonds, I., and K. Keay (2009), Extraordinary September Arctic sea ice reductions and their relationships with storm behavior over 1979–2008, *Geophys. Res. Lett.*, *36*, L19715, doi:10.1029/2009GL039810.

Steele, M., J. Zhang, and W. Ermold (2010), Mechanisms of summertime upper Arctic Ocean warming and the effect on sea ice melt, *J. Geophys. Res.*, *115*, C11004, doi:10.1029/2009JC005849.

Stroeve, J., L. C. Hamilton, C. M. Bitz, and E. Blanchard-Wrigglesworth (2014), Predicting September sea ice: Ensemble skill of the SEARCH Sea Ice Outlook 2008–2013, *Geophys. Res. Lett.*, *41*, 2411–2418, doi:10.1002/2014GL059388.

Stroeve, J. C., V. Kattsov, A. Barrett, M. Serreze, T. Pavlova, M. Holland, and W. N. Meier (2012), Trends in Arctic sea ice extent from CMIP5, CMIP3 and observations, *Geophys. Res. Lett.*, *39*, L16502, doi:10.1029/2012GL052676.

Sun, W., N. G. Loeb, R. Davies, K. Loukachine, and W. F. Miller (2006), Comparison of MISR and CERES top-of-atmosphere albedo, *Geophys. Res. Lett.*, *33*, L23810, doi:10.1029/2006GL027958.

Wang, W., M. Chen, and A. Kumar (2013), Seasonal prediction of Arctic sea ice extent from a coupled dynamical forecast system, *Mon. Weather Rev.*, *141*(4), 1375–1394, doi:10.1175/MWR-D-12-00057.1.

Woodgate, R. A., T. Weingartner, and R. Lindsay (2010), The 2007 Bering Strait oceanic heat flux and anomalous Arctic sea-ice retreat, *Geophys. Res. Lett.*, *37*, L01602, doi:10.1029/2009GL041621.

Zhang, J., R. Lindsay, M. Steele, and A. Schweiger (2008), What drove the dramatic retreat of arctic sea ice during summer 2007?, *Geophys. Res. Lett.*, *35*, L11505, doi:10.1029/2008GL034005.